A Novel Highly Efficient Torque Sharing Algorithm for Dual Stator Winding Induction Machines for Various Speed Regions

M. Ayaz Khoshhava, H. Abootorabi Zarchi, G.R. Arab Markadeh, H.R. Mosaddegh and K. Al-Haddad. *IEEE Life Fellow*

***Abstract*—This paper proposes a novel and highly efficient torque-sharing algorithm for DSWIMs. This algorithm introduces three modes of operation for DSWIMs based on the command speed and the required load power. Implementing this algorithm makes the accurate flux calculation and control possible in very low speed regions, including zero speed. In higher speed regions, if one of the winding sets is able to supply the required power solely, the other is switched off to augment the overall efficiency. In higher required powers, both winding sets cooperate to supply the load torque and the required electromagnetic torque division between the two winding sets is fulfilled based on their power ratings. This guarantees for overloading avoidance in various operation conditions. Moreover, the optimal flux condition is guaranteed in various speed regions free of the torque - sharing. In addition, this algorithm is general and can be implemented in direct torque control and field-oriented control schemes in various reference frames. The proposed algorithm has been experimentally implemented in a 3.3kW vector controlled DSWIM drive system. In this flux and speed control system, the flux is controlled such that a search based Maximum Torque per Ampere (MTPA) algorithm is realized. The proposed MTPA strategy is insensitive to DSWIM parameters and the load variations. The experimental results confirm the functionality of the proposed DSWIM drive system in various operation conditions.**

***Index Terms*—Dual Stator Winding Induction Machines (DSWIMs), Torque sharing, zero speed region operation, Maximum Torque per Ampere (MTPA).**

NOMENCLATURE

V, I, λ	Voltage, current, flux
$\omega_i, \omega_r, \omega_{sl}$	Synchronous, rotor, slip speeds
R and L	Resistance and inductance
P	Number of poles
T_e, T_L	Electromagnetic, load torques
J	Moment of inertia
B	Friction coefficient
P_e, P_{conv}	Electric and converted powers
P_{cu}	Copper loss
k_P, k_I	Proportional and integral gains of the speed controller
θ	Transformation angle
B_{gi}	The amplitude of the flux density of the ith winding set
Superscripts	
Star (*)	Reference value
Prime (′)	Rotor parameter referred to stator
Subscripts	
s, r, m	Stator, rotor and mutual
ABC, XYZ	Two pole and six pole windings
i=1, 2	*ABC* and *XYZ*

I. Introduction

THREE phase Induction Machines (IMs) due to their significant advantages over other sorts of electrical machines consist a major part of the electrical machines utilized in the world industry [1]. These advantages can be addressed as involving low fabrication and maintenance costs, high reliability and the ability of operating in various environmental conditions [2]. Despite these valuable advantages, the operation of IMs has some difficulties in very low and zero speed regions, specifically in the sensor-less applications [3]. In the zero-speed region, in order to avoid flux saturation, the stator voltage must be decreased significantly. As a result, the voltage drop on the stator resistance is not negligible anymore and its effect must be taken into consideration for the flux estimation. However, this resistance is not constant and it is operating point dependent. Moreover, in this operation region because of the interference between higher band frequencies of dc-rejection filter with low-pass filter of the stator currents, the dc-offset of measured currents may distort the true values of stator fluxes [4]. Therefore, IM drives will encounter some limitations in this region.

In 1998 Lipo et. al introduced a new type of dual winding IM, in which the zero speed operation complexities have been eliminated [5]. The stator of these IMs, called Dual Stator Winding IMs (DSWIMs), includes two sets of three phases windings with different pole pairs and their rotor is of the squirrel cage type. Therefore, there is no direct and indirect coupling between the stator winding sets [6]. Some of DSWIMs advantages over other sorts of IMs are enumerated as:

- Despite Brushless Doubly Fed IMs (BDFIMs), which adopted rotors with special structure called nested-loop, they can be fabricated by utilizing the commercially available IM squirrel cage rotors. Thus, they involve lower fabrication costs [7].
- Ability to operate in a broader speed region in comparison to BDFIMs, including zero speed region [8].
- In case of 1:3 pole pair combination, the magnetomotive force will be approximately trapezoidal. This results in better iron utilization in comparison to standard IMs [9].
- In spite of the conventional dual stator winding IMs with equal pole pairs for both winding sets, the control of

winding sets in these types of DSWIMs is independent from each other. This results in simpler control structure and zero speed operation capability [10] and [11].

According to the above-mentioned advantages of DSWIMs, they have been proposed both for generating and motoring applications. In [12] a highly efficient control scheme has been proposed for DSWIMs that has been adopted to create a DC power supply in two modes: paralleled and series windings. This control system is based on the Input Output Feedback Linearization (IOFL) method, which is highly dependent on machine model and its parameters. In this paper, the loss minimization has been fulfilled through a model-based method, which determines the optimal power partition factor between the two winding sets. A DSWIM control methodology has been proposed in [13] for a generator-rectifier system. In this system, the rectified output voltages are controlled such that the copper losses are minimized. This method is also based on the machine accurate parameters. Another DSWIM control system has been proposed in [14] for the generating application. This sensorless system has been designed for a wind energy harvesting system.

In addition to the generating, DSWIMs have been interesting for the motoring application. In [6], the concept of DSWIM speed control has been addressed for the motoring application based on an Indirect Field Oriented control (IFOC) system. Another IFOC based speed control has been introduced in [15] for DSWIMs. This control scheme is free of speed sensors, in which the speed is estimated through a Model Reference Adaptive System (MRAS). The speed sensorless control of DSWIMs has also been addressed in [16]. In this system the speed and flux has been done through an emotional controller.

Besides the speed and flux, the electromagnetic torque control for DSWIMs is of significant importance. Since, there are two sources of electromagnetic torque generation. Accordingly, the electromagnetic torque sharing must be such that no overloading occurs for winding sets. In addition, the optimal operation condition must be satisfied. Already, in [17-19] a torque-sharing algorithm has been introduced for DSWIMs. In the proposed algorithm, the load torque is divided between the two winding sets such that the optimal relative position is guaranteed for winding fluxes. Although, this results in optimal DSWIM iron utilization, the stator windings may experience overloading. However, in [20] it is declared that the relative position of DSWIM winding fluxes can be fixed at its optimal value through proper reference frame angle determination and free of the torque sharing. In addition, this algorithm is not implementable in very low and zero speed regions. In [21-24], another torque-sharing algorithm has been introduced for DSWIM, which is implementable in various speed regions. This algorithm has two modes of operation: the synchronous and asynchronous. In the synchronous mode two windings sets cooperate to supply the load torque based on their power ratings and the asynchronous mode has been designed such that the flux estimation fulfilled appropriately in zero speed region.

In this paper, a novel torque-sharing algorithm is proposed. This algorithm decreases the DSWIM losses by introducing a new mode of operation. Indeed, this algorithm not only has the advantages of the torque sharing technique proposed in [21-24], but also increases the overall efficiency of the DSWIM drive system. The superiorities of the proposed torque sharing algorithm can be addressed as follows:

- Guaranteeing the optimal flux position and overload avoidance of each winding sets.
- Higher efficiency; since, one of the winding sets is switched off during the low load condition.
- Implementable in various control schemes such as Direct Torque Control (DTC) and Field Oriented Control (FOC) in different reference frames.

Moreover, in this control system, a novel MTPA technique is proposed for DSWIMs drives. The proposed method is search-based and compared with the model-based MTPA strategies, benefits from the following advantages:

- It is independent of all the motor parameters while the model-based MTPA methods are based on most of the motor parameters, which must be accurately identified.
- In contrast to the model-based MTPA strategies, in which iron losses are generally neglected, the proposed MTPA control considers the effect of iron losses since the measured current is being employed in the search process.
- Implementable for various load torque profiles attached to the motor shaft.

II. DSWIM Electrical Model

The stator and rotor voltage equations for the each of the winding sets of a DSWIM are as follows [5]:

$$V_{dsi} = R_{si} I_{dsi} + \frac{d\lambda_{dsi}}{dt} - \omega_i \lambda_{qsi} \tag{1}$$

$$V_{qsi} = R_{si} I_{qsi} + \omega_i \lambda_{dsi} + \frac{d\lambda_{qsi}}{dt} \tag{2}$$

$$V'_{dri} = R'_{ri} I'_{dri} + \frac{d\lambda'_{dri}}{dt} - (\omega_i - \omega_r)\lambda'_{qri} = 0 \tag{3}$$

$$V'_{qri} = R'_{ri} I'_{qri} + \frac{d\lambda'_{qri}}{dt} + (\omega_i - \omega_r)\lambda'_{dri} = 0 \tag{4}$$

where:

$$\lambda_{dsi} = L_{si} I_{dsi} + L_{mi} I'_{dri} \tag{5}$$

$$\lambda_{qsi} = L_{si} I_{qsi} + L_{mi} I'_{qri} \tag{6}$$

$$\lambda'_{dri} = L_{mi} I_{dsi} + L'_{ri} I'_{dri} \tag{7}$$

$$\lambda'_{qri} = L_{mi} I_{qsi} + L'_{ri} I'_{qri} \tag{8}$$

The electromagnetic torques produced by the *ABC* and *XYZ* winding sets are calculated as (9) and (10), respectively.

$$T_{e1} = \frac{3}{4} P_1 I_{qs1} \lambda_{ds1} = k_1 I_{qs1} \lambda_{ds1} \tag{9}$$

$$T_{e2} = \frac{3}{4} P_2 I_{qs2} \lambda_{ds2} = k_2 I_{qs2} \lambda_{s2} \tag{10}$$

The electromagnetic torque of a DSWIM is sum of the electromagnetic torques produced by each winding set. Consequently, the mechanical equation is as follows:

$$T_{e1} + T_{e2} - T_L = J \frac{d\omega_r}{dt} + B\omega_r \tag{11}$$

III. The Proposed Torque Sharing Algorithm

The flowchart of the proposed torque-sharing algorithm is depicted in Fig.1. As it is illustrated, this algorithm involves three modes of operation: the asynchronous, synchronous and single winding modes. The activation of each of these operation modes is free of the load nature and it is based on the reference speed and the required converted power, which is defined as the product of the electromagnetic torque and the rotor speed. Actually, if the reference rotor speed is lower than a minimum value (ω_{min}), the asynchronous operation mode is activated. Otherwise, the reference total electromagnetic torque is determined based on the rotor speed error ($e_\omega = \omega_r^* - \omega_r$). Generally, in vector control and direct torque control schemes, the reference torque is the output of the speed regulator. If a Proportional Integral (PI) controller is adapted as the speed regulator, T_e^* equals:

$$T_e^* = e_\omega \left(k_P + \frac{k_I}{s} \right) \tag{12}$$

Then, the reference converted power is calculated as (13).

$$P_{conv}^* = T_e^* \omega_r^* \tag{13}$$

If the converted power is higher than the rated power of PW, the DSWIM operates in the synchronous mode. Else ways, the CW is switched off and the PW supplies the load singly. It can be shown that this way the DSWIM losses are reduced. Considering the power as the product of the speed and torque, according to the above discussions, the permissible region of operation in the torque-speed plane in various of the operation modes can be illustrated as Fig. 2. Although, this algorithm can be adapted for various reference frames, the formulations given in this part are derived for the stator flux-oriented frame as an example. The following introduces various operation modes in more details.

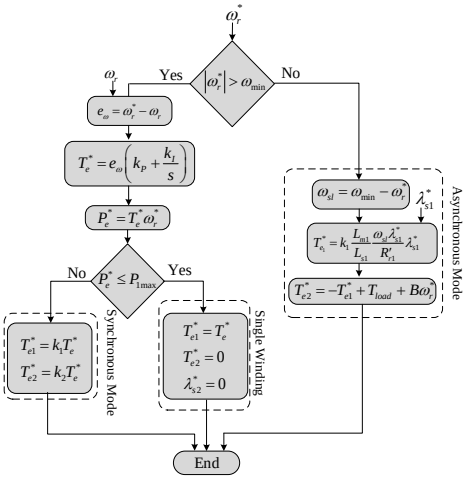

Fig. 1. The flowchart of the proposed torque-sharing algorithm

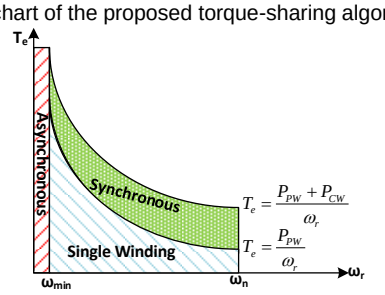

Fig. 2 The proposed DSWIM drive system

A. The Asynchronous Operation Mode

This mode of operation pertains to the very low speed regions, where the reference speed is lower than ω_{min}. In this mode, in order to conveniently estimate the winding fluxes, the frequency of one of the low-pole winding, is fixed at ω_{min}. Assume $p_1 < p_2$, the stator q-axis flux of the PW equals:

$$\lambda_{qs1} = L_{s1} I_{qs1} + L_{m1} I'_{qr1} \tag{14}$$

In the stator flux-oriented reference frame $\lambda_{qs1} = 0$ and $\lambda_{ds1} = \lambda_{s1}$. Accordingly, the stator q-axis current will be:

$$I_{qs1} = \frac{-L_{m1}}{L_{s1}} I'_{qr1} \tag{15}$$

Let's consider *i=1* in (4) and assume $d\lambda'_{qr1}/dt = 0$ in the steady-state condition, I'_{qr1} equals:

$$I'_{qr1} = \frac{-\omega_{sl} \lambda'_{dr1}}{R'_{r1}} \tag{16}$$

where $\omega_{sl} = \omega_{\min} - \omega_r^*$. If the leakage flux is neglected, $\lambda_{ds1} = \lambda'_{dr}$. Then substituting (16) into (15), I_{qs1} is approximately:

$$I_{qs1} \approx \frac{L_{m1}}{L_{s1}} \frac{\omega_{sl} \lambda_{ds1}}{R'_{r1}} \tag{17}$$

Thus, the reference electromagnetic flux of this winding set in the stator flux reference frame equals:

$$T_{e1}^* = k_1 \frac{L_{m1}}{L_{s1}} \frac{\omega_{sl} \lambda_{s1}^*}{R'_{r1}} \lambda_{s1}^* \tag{18}$$

Consistent with (11), the reference electromagnetic torque of the *XYZ* winding set in the steady-state condition will be:

$$T_{e2}^* = -T_{e1}^* + T_L + B\omega_r^* \tag{19}$$

B. The Synchronous Operation Mode

As previously discussed, this mode of operation will be activated, if the reference speed is more than ω_{min} and the reference converted power is higher than the rated power of PW, where both windings cooperate to supply the load. In this condition, the winding fluxes can be estimated properly. Thus, the flux optimization strategies are implementable for DSWIMs. The main condition for these strategies is the flux synchronization [20]. Accordingly, in order to synchronize the winding fluxes, their frequency must have the same ratio as their pole pair ratio. The electrical power produced by each of the winding sets equals:

$$P_{ei} = T_{ei} \omega_e \tag{20}$$

As the electrical speed is equal for both winding sets, the electrical power ratio of winding sets is equal to their torque ratio. Thus, in this mode of operation, in order to avoid overloading of winding sets, the electromagnetic torque is shared between them according to their power ratings. If the ratio of the nominal power of the ith winding set to the total power of a DSWIM is represented by k_i, the reference torque of each winding set equals:

$$T_{ei}^* = k_i T_e^* \tag{21}$$

C. Single Winding Operation Mode

As it is discussed before, this mode of operation pertains to the conditions in which, $\omega_r^* > \omega_{\min}$ and $P_{conv}^* < P_{1\max}$. Indeed, in

this condition PW is able to supply the required load torque and the DSWIM is operating as a conventional three phase Induction Machine (IM). As the CW, the frequency of which is three times higher than that of PW, is switched off, the DSWIM iron losses are lower in comparison to the synchronous operation mode. To compare the copper losses in the single winding and synchronous modes, let's assume the required power is lower than the PW nominal power and its ratio to the DSWIM rated power equals *k* and the ratio of the nominal power of the PW and CW to the DSWIM rated power is represented by k_1 and k_2, respectively. Two scenarios are considered:

1) Both windings cooperate to supply the required power.

2) PW supplies the required power singly.

The relevant copper losses are shown by P_{cu1} and P_{cu2} and if the load power ratio of an IM to the nominal power is *k*, the relative copper losses is proportional to the nominal copper losses by k^2. Accordingly, P_{cu1} and P_{cu2} are calculated as:

$$P_{cu1} = R_{s1}\left(k/k_1\right)^2 I_{s1}^2 \tag{22}$$

$$P_{cu2} = R_{s1}k^2 I_{s1}^2 + R_{s2}k^2 I_{s2}^2 \tag{23}$$

The parameters and nominal values of the DSWIM under study are tabulated in table I. substituting the parameters given table I in (22) and (23), P_{cu1} and P_{cu2} are determined as:

$$P_{cu1} = 85.2k^2 \qquad P_{cu2} = 89.06k^2$$

It is clear that $P_{cu1} < P_{cu2}$ and as a result the copper losses in the single winding operation mode are lower than that of synchronous operation mode. Accordingly, if the required power is not higher than PW rated power, switching off the CW increases the overall DSWIM efficiency. In this condition: $T_{e1}^* = T_e^*;\ T_{e2}^* = 0;\ \lambda_{s2}^* = 0$.

IV. The Proposed DSWIM Drive System

The proposed drive system for a DSWIM with p_1 (*ABC*) and p_2 (*XYZ*) number of poles is depicted in Fig.3. This drive system is a vector control scheme in the stator flux-oriented reference frame. In this system, the torque-sharing algorithm determines the reference electromagnetic torques for each winding set according to the rotor speed and its reference command.

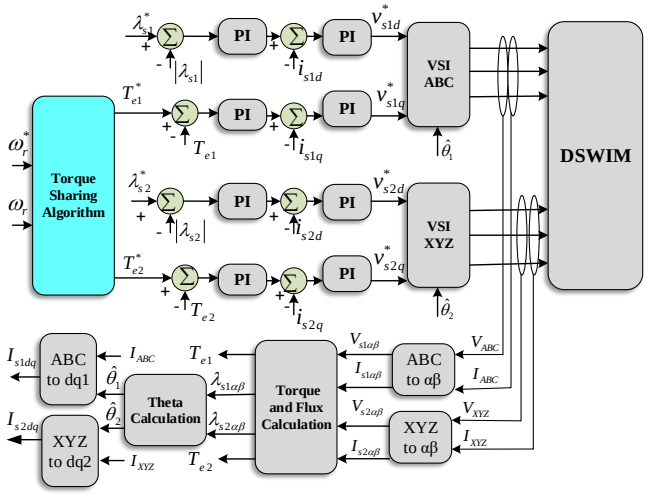

Fig. 3. The proposed DSWIM drive system

TABLE I
DSWIM Nominal Values and Parameters

Parameter	Value	
	ABC	***XYZ***
Pole number	2	6
Output Power	2830W	500W
Voltage Frequency	50 Hz	150 Hz
RMS Line Voltage	230 V	80 V
RMS Phase Current	9A	5 A
R_s	0.76 Ω	1.1Ω
R_r'	0.684Ω	0.66Ω
L_{ms}	122.5 *mH*	15.83 *mH*
L_{ls}	3.565 *mH*	1.505 *mH*
L_{lr}'	3.565 *mH*	1.505 *mH*
Rotor Speed	2850 rpm	
Efficiency	88%	
Nominal Torque	11.15N.m	

The reference torques are compared with the calculated ones. The resultant errors pass through *PI* controllers and consist the reference q-axis currents. The errors between these currents and the measured ones are fed to the respective *PI* controllers, the output of which is the reference q-axis voltages for the Voltage Source Inverters (VSIs). Similar procedure is fulfilled for the d-axis voltage determination, except that, the deference between the reference fluxes and the calculated ones are passed through the related *PI* controllers which regulate the reference d-axis currents. Figure 4 depicts the reference frame determination algorithm. As it is illustrated, in the proposed DSWIM drive system, the reference frame angles determination is fulfilled in agreement with the torque-sharing technique. The reference frame angles for each winding set in various operation modes are calculated as follows.

A. The Asynchronous Operation Mode

As discussed earlier, if the reference speed is lower than ω_{min}, the asynchronous operation mode is recognized. In this condition, the frequency of *PW* is kept at a constant value (ω_{min}). Accordingly:

$$\theta_1 = \int \omega_{\min} dt \tag{24}$$

In this mode of operation there is no synchronization between the winding fluxes and the reference frame angle of *CW* is determined independently.

$$\theta_2 = \tan^{-1}\left(\lambda_{s\beta 2}/\lambda_{s\alpha 2}\right) \tag{25}$$

A. The Synchronous Operation Mode

If the reference speed is above ω_{min} and PW is not able to provide the required converted power, this mode is activated. In [20] it is declared that in the optimal flux condition the winding fluxes must be synchronized and their relative position must be kept at 180° ($\delta_{optimal}=180$). To guarantee this criterion in this mode of operation, a similar method is implemented, which involves the reference frame angle compensation. Figure 5 illustrates the block diagram of the reference frame angle determination method in the synchronous operation mode.

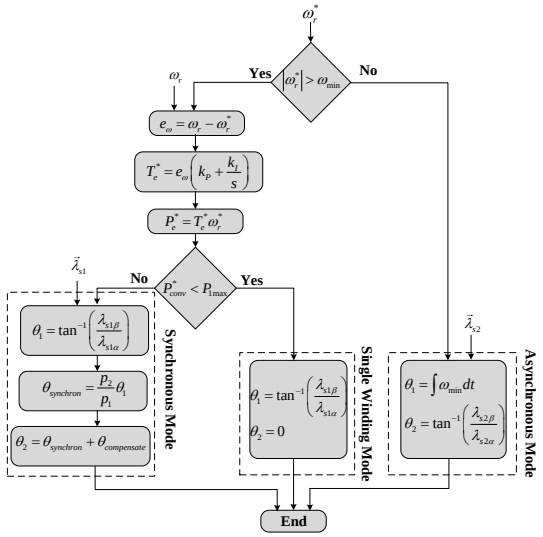

Fig. 4. The proposed reference frame determination algorithm

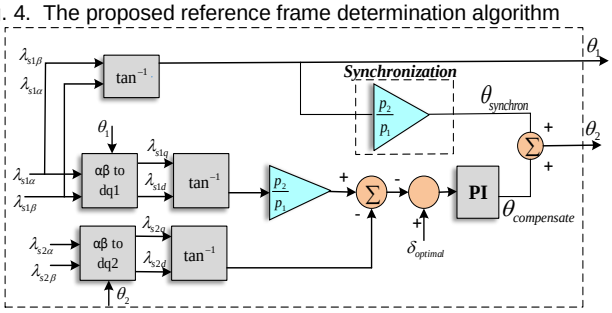

Fig. 5. Reference frame angle determination in synchronous operation mode [20].

As it is illustrated, in this mode, the reference frame angle of PW ($\tan^{-1}(\lambda_{s\beta1}/\lambda_{s\alpha1})$) is multiplied by the pole pair ratio to determine $\theta_{synchronous}$.

$$\theta_{synchron} = \frac{p_2}{p_1}\tan^{-1}\left(\lambda_{s\beta1}/\lambda_{s\alpha1}\right) \tag{26}$$

This angle is summed up with a compensation angle, which guarantees the optimal relative position to determine the reference frame angle for CW.

$$\theta_2 = \theta_{synchron} + \theta_{compensate} \tag{27}$$

C. The Single Winding Operation Mode

This mode pertains to the condition that the required power is lower than PW rated power. In this mode CW is switched off, thus its reference frame angle is set at zero ($\theta_2 = 0$). The reference frame angle for PW is calculated similar to (25) as:

$$\theta_1 = \tan^{-1}\left(\lambda_{s\beta1}/\lambda_{s\alpha1}\right) \tag{28}$$

V. Proposed MTPA Algorithm

In the proposed DSWIM drive system, the reference fluxes for each winding set are determined such that an MTPA algorithm is realized. The flowcharts of the proposed search based MTPA algorithm and the start fluxes determination method are depicted in Figs. 6 (a) and (b). This algorithm is realized in the steady-state condition. Accordingly, consistent with Fig. 6(a), continuously the speed is compared with its

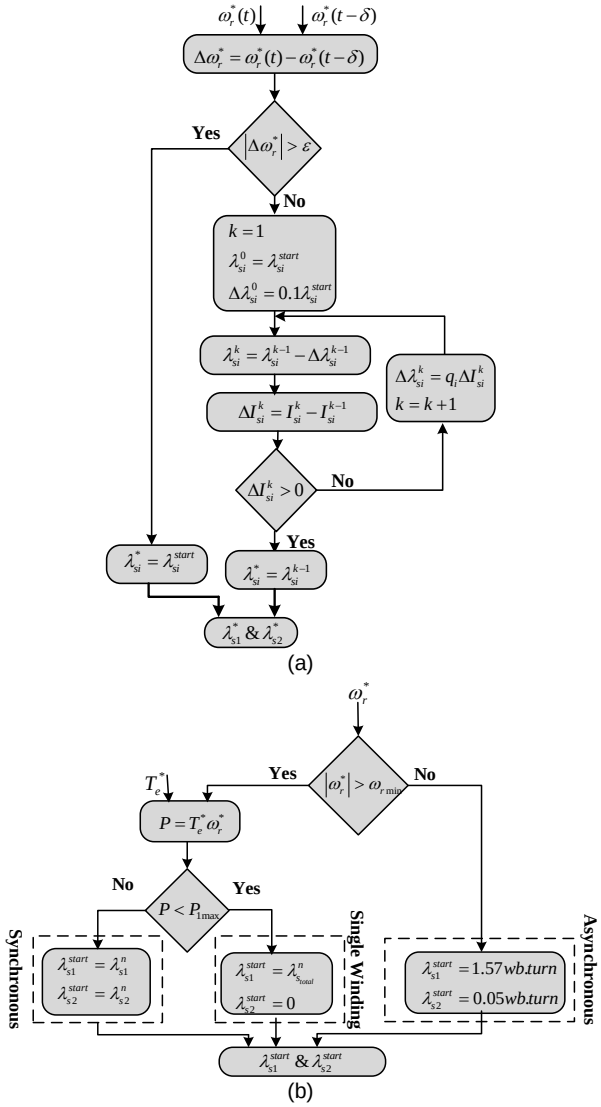

Fig. 6. MTPA algorithm a) whole system b) start flux determination

value in δ samples before. If the error is higher than ε, the transient condition is recognized and the reference fluxes are set to their start values. Otherwise, the algorithm searches for the optimum flux references. This prevents under fluxing. Since, in the case of under-fluxing, the machine will not be in the steady-state condition and the algorithm sets the flux again at its start value to prevent any instability. The reference flux of each winding set is reduced step wisely from λ_{si}^{start}. In each step the stator current variation (ΔI_{si}^{k}) is measured. If $\Delta I_{si}^{k} < 0$, the search process continues. Otherwise, the optimum value of flux will be that of the previous step. As the flux is decreased from the start value in the search process, the upper boundary for the winding fluxes is their start value. The lower boundary in the optimization process is determined automatically in the optimization process. Indeed, the lower boundary is the optimal value determined through the search process. If the flux goes lower than this value, the current will increase, which results in setting the flux again at the optimal value.

It is worth noting that the alteration of flux in the proposed algorithm is done via variable steps proportional to the current reduction. This, increases the accuracy and the implementation

speed. Figure 6(b) illustrates the start fluxes determination strategy for the MTPA algorithm. The start flux in each operation mode is as follows.

A. Asynchronous Operation Mode

In this mode, where the windings fluxes vectors are rotating with unequal speeds, one can write:

$$B_{t\max} = B_{g1} + B_{g2} \tag{29}$$

As the rotor speed is relatively low in this operation mode and B has also a low value, one can omit ($B\omega$) from (19). Based on this assumption and (18), (19) can be rewritten as (30).

$$T_{e2}^{*} = -k_1 \frac{L_{m1}}{L_{s1}} \frac{\omega_{sl}}{R'_{r1}} \left(\lambda_{s1}^{*}\right)^2 + T_{load} = -k' \left(\lambda_{s1}^{*}\right)^2 + T_{load} \tag{30}$$

In (30), $k' = k_1 (L_{m1}\omega_{sl} / L_{s1}R'_{r1})$. According to (30) and (10), i_{sq2} and accordingly i_{sd2} can be calculated as (31) and (32), respectively.

$$i_{sq2} = \frac{k' \left(\lambda_{s1}\right)^2 - T_{load}}{k_2 \lambda_{s2}} \tag{31}$$

$$i_{sd2} = \sqrt{i_{s2}^2 - \left(\frac{k' \left(\lambda_{s1}\right)^2 - T_{load}}{k_2 \lambda_{s2}}\right)^2} \tag{32}$$

Let the derivative terms in (3) and (4) be zero in the steady-state condition, the rotor currents can be determined as:

$$i'_{rd2} = \frac{\omega_{sl2}}{R'_{r2}} \lambda'_{rq2} \tag{33}$$

$$i'_{rq2} = -\frac{\omega_{sl2}}{R'_{r2}} \lambda'_{rd2} \tag{34}$$

Based on (33) and (34), one can write:

$$i'_{rd2} = \frac{-i'_{rq2}}{\lambda'_{rd2}} \lambda'_{rq2} \tag{35}$$

According to (5-8), (35) can be rewritten as (36).

$$i'_{rd2} = \frac{\left(L_{s2} - \frac{L'_{r2}L_{s2}^2}{L_{m2}^2}\right)}{L_{m2} i_{sd2} + L'_{r2} i'_{rd2}} i_{sq2}^2 \tag{36}$$

If both sides of (36) are multiplied by $L_{m2} i_{sd2} + L_{s2} i'_{rd2}$, there will be a second order equation in terms of i'_{rd2}, which can be solved as (37).

$$i'_{rd2} = \frac{-\frac{L_{m2}}{L'_{r2}} i_{sd2} \pm \sqrt{\left(\frac{L_{m2}}{L'_{r2}}\right)^2 i_{sd2}^2 + 4\left(L_{s2} - \frac{L'_{r2}L_{s2}^2}{L_{m2}^2}\right) i_{sq2}^2}}{2} \tag{37}$$

Substituting (37) in (5) results in (38).

$$\lambda_{s2} = \left(L_{s2} - \frac{L_{m2}^2}{L'_{r2}}\right) i_{sd2} + L_{m2} \left(\frac{\sqrt{\left(\frac{L_{m2}}{L'_{r2}}\right)^2 i_{sd2}^2 + 4\left(L_{s2} - \frac{L'_{r2}L_{s2}^2}{L_{m2}^2}\right) i_{sq2}^2}}{2}\right) \tag{38}$$

According to (32), (38) can be rewritten as (39).

$$\lambda_{s2} = \left(L_{s2} - \frac{L_{m2}^2}{L'_{r2}}\right) \sqrt{i_{s2}^2 - \left(\frac{k' \left(\lambda_{s1}\right)^2 - T_{load}}{k_2 \lambda_{s2}}\right)^2} + L_{m2} \sqrt{\left(\frac{L_{m2}}{2L'_{r2}}\right)^2 i_{s2}^2 + \left(\left(L_{s2} - \frac{L'_{r2}L_{s2}^2}{L_{m2}^2}\right) - \left(\frac{L_{m2}}{L'_{r2}}\right)^2\right) \left(\frac{k' \left(\lambda_{s1}\right)^2 - T_{load}}{k_2 \lambda_{s2}}\right)^2} \tag{39}$$

Considering a linear relation between λ_{si} and B_i as $\lambda_{si} = m_i B_i$ and substituting B_1 from (29) in (39) to maximize the iron utilization, results in (40). It is worth noting that m_i can be determined according to the nominal voltage and frequency of each winding set [6].

$$k_2 (m_2 B_2)^2 = \left(L_{s2} - \frac{L_{m2}^2}{L'_{r2}}\right) \sqrt{k_2 (m_2 B_2)^2 i_{s2}^2 - \left(k' m_1^2 \left(B_{\max} - B_2\right)^2 - T_{load}\right)^2} + L_{m2} \sqrt{\left(\frac{L_{m2}}{2L'_{r2}}\right)^2 k_2 (m_2 B_2)^2 i_{s2}^2 + \left(\left(L_{s2} - \frac{L'_{r2}L_{s2}^2}{L_{m2}^2}\right) - \left(\frac{L_{m2}}{L'_{r2}}\right)^2\right) \left(k' m_1^2 \left(B_{\max} - B_2\right)^2 - T_{load}\right)^2} \tag{40}$$

The value of starting fluxes in this condition are determined such that the maximum electromagnetic torque can be supplied to have an appropriate dynamic performance. Accordingly, from (40), T_{load} is derived as a function of B_2 and let its derivative be zero (and let its derivative be zero). This way, the value of B_2 is determined. Based on (29), B_1 is also determined. Based on the DSWIM parameters given in [17], the start values for CW and PW fluxes equal to $\lambda_{s1}^{start} = 1.57$ and $\lambda_{s2}^{start} = 0.05$, respectively. It is worth noting that these fluxes values are considered just for the start of the asynchronous operation mode and the optimal flux values in this operation mode, which minimize the stator currents for the required load torque are determined through the search algorithm.

Consistent with (18), the flux reduction in PW leads to reduction in its reference torque. According to (19), this torque reduction reduces the reference torque of CW, too. Considering a constant value for the CW reference flux, the torque reduction results in its current reduction. Consequently, in asynchronous operation mode, the flux search in PW influences the currents of both windings sets. As a result, in this mode, the flux of CW is set to a constant value. The flux of PW is varied and the total current (sum of the amplitudes of CW and PW currents) is analyzed.

B. Synchronous Operation Mode

In this mode the start flux for each winding set is equal to the rated flux value of that winding.

C. Single Winding Operation Mode

The start flux for the CW is set to zero and that of PW is set to the total permissible flux value for DSWIM ($\lambda_{S_{total}}^{n}$). Since, in this mode of operation, just PW is on.

VI. Experimental Results

The proposed drive system is implemented for a 3.3kW DSWIM with the specifications given in table I. Consistent with the nominal powers given in this table, k_1 and k_2 are 0.85 and 0.15, respectively. In this system, ω_{min} is 5 rad/s, which is one twenties of rated synchronous speed, as it is done and recommended in [6]. Figure 7 illustrates the experimental test bench. As it is illustrated, in this system the *ABC* and *XYZ* winding sets are fed through two independent VSIs. The line currents of each winding set are measured via their associated current senor boards, each of which includes three LEM LA55P current sensors. In addition, this DSP-based drive system is provided with four LEM LV-25-P voltage sensors

for measuring the windings line voltages. The main module of this system is the TMS320F28335 signal processor board, which generates all control commands. A 1024 pulse incremental encoder provided by the OPCKON Co. measures the rotor speed. In this system, a DC generator is employed as the mechanical load. This generator supplies a resistive load. Therefore, the DSWIM load torque has an approximately linear relation with the rotor speed. In general, the emf produced in a DC generator has an approximately linear relation with its rotor speed. Accordingly, if the DC generator losses are neglected, the electromagnetic torque and the armature voltage can be calculated as (41) and (42), respectively:

$$T_R = \frac{P_r}{\omega_r} = \frac{V_{ar}^2}{R_L \omega_r} \tag{41}$$

$$V_{ar} = k_{ar} \Phi_{DC} \omega_e \tag{42}$$

where, k_{ar} is a constant value and R_L and V_{ar} stand for the load resistance and the armature voltage, respectively. It is clear that Φ_{DC} ,the flux of the DC generator, will be constant through maintaining the excitation voltage constant. For a DC generator with p poles, one can rewrite (42) as:

$$V_{ar} = k_{ar} \Phi_{DC} \frac{p}{2} \omega_r \tag{43}$$

Substituting the armature voltage from (43) into (41) results in:

$$T_R = \frac{\left(k_{ar} \Phi_{DC} \frac{p}{2}\right)^2}{R_L} \omega_r = k^* \omega_r \tag{44}$$

where, $k^* = \dfrac{\left(k_{ar} \Phi_{DC} \frac{p}{2}\right)^2}{R_L}$.

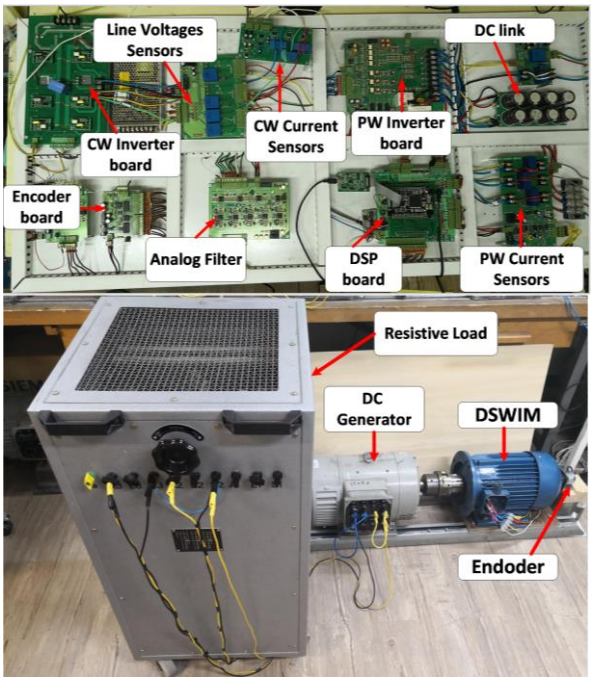

Fig.7. The experimental test bench

Figures 8-15 illustrate the experimental results. The rotor speed and its reference command are shown in Fig. 8 (a). Consistent with this figure, this speed profile includes asynchronous, synchronous and single winding operation modes. The speed controller can control the speed in various regions and operation modes accurately and with satisfactory dynamics. Figures 8 (b) and (c) illustrate the fluxes of the PW and CW and their reference commands, respectively. According to these figures, in the asynchronous operation mode, the first four seconds of the test, the PW flux is fixed at 0.05 wb.turn. After the determination of the constant speed at t=0.6sec, the search process begins for PW flux. After five steps, the optimal value for this flux (0.1 wb.turn) is specified. It worth noting that, since the load torque in this condition is very low, the flux has a relatively low value in this operation mode. After the termination of the asynchronous operation mode, the single winding mode is determined at t=4.1sec. In this mode the CW reference flux is zero and as the speed is varying, the reference flux for PW is set to 1.73 wb.turn. At t=6.9 sec, DSWIM enters the synchronous operation mode and reference fluxes for PW and CW are set to 1.98 wb.turn and 0.11 wb.turn, respectively. Upon the constant condition for speed is recognized at t=7.2 sec, the search process for the

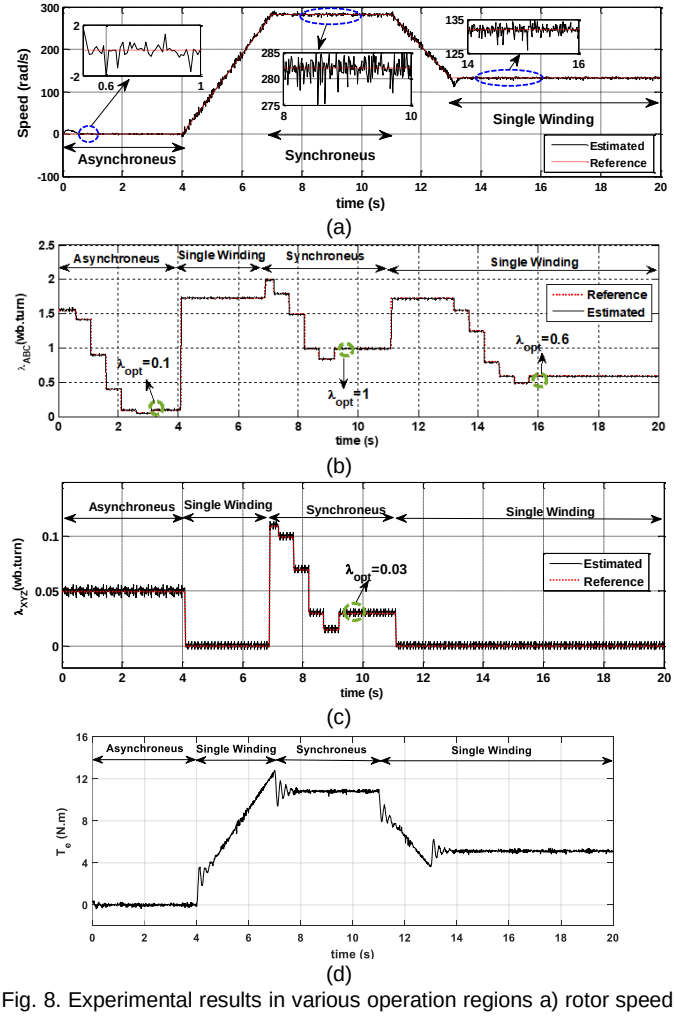

Fig. 8. Experimental results in various operation regions a) rotor speed b) *PW* flux b) CW flux d) electromagnetic torque

This article has been accepted for publication in IEEE Transactions on Industrial Electronics. This is the author's version which has not been fully edited and content may change prior to final publication. Citation information: DOI 10.1109/TIE.2023.3286002

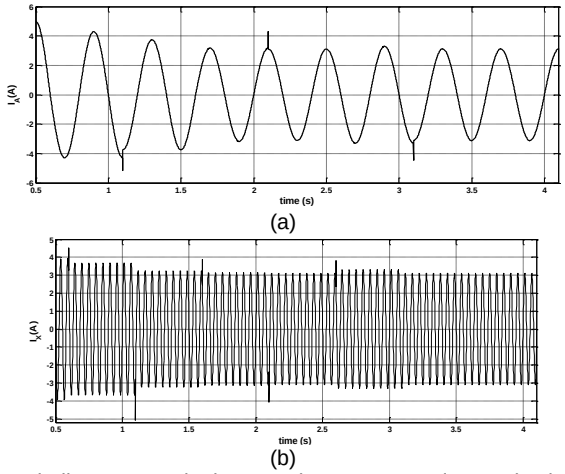

Fig. 9. Winding currents in the asynchronous operation mode a) PW b) CW

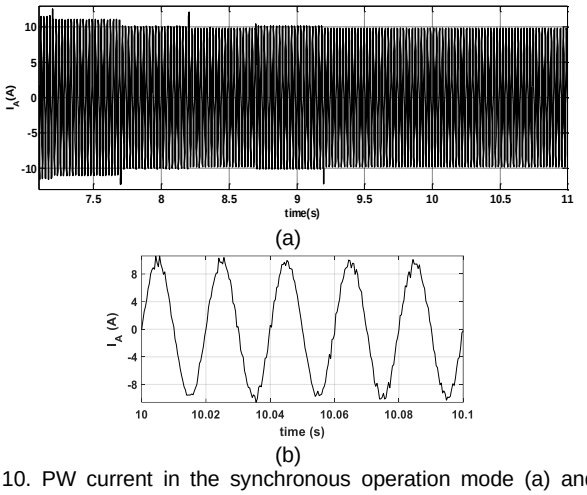

Fig. 10. PW current in the synchronous operation mode (a) and its zoomed (b) waveforms

both winding sets starts. After 3 and 4 steps, the optimal fluxes are determined respectively for the PW and CW and the winding fluxes are set at these optimal values until the end of synchronous operation mode. At t=11.1 sec by speed reduction, DSWIM goes to single winding again and PW and CW fluxes are set to 1.73 and zero, respectively. After 2.1 sec, the speed reaches to steady-state condition and the optimal flux search process for PW is initiated. Consistent with Fig. 8 (b), the optimal flux is determined in 5 steps, which is 0.6 wb.turn. The total electromagnetic torque has been illustrated in Fig. 8 (d). Consistent with (44) the electromagnetic torque has a similar shape to the rotor speed and as it is expected there are some transient oscillations during the mode changes. The current waveforms of the phase A of PW and phase X of CW in the asynchronous operation mode are illustrated in Figs. 9 (a) and (b), respectively. The THD of the currents of phase A and X in this mode of operation are 0.5% and 0.58%, respectively. Similar current and their zoomed waveforms for the synchronous operation mode are depicted in Figs. 10 and 11. The THD of the currents shown in Figs. 10 and 11 are 4.9% and 3.2%, respectively.

Figure 12 depicts the phase difference between the PW and CW flux vectors ($\Delta\theta$) in the synchronous mode. According to this figure, $\Delta\theta$ is 180° during this operation mode, which guarantees the optimal flux condition.

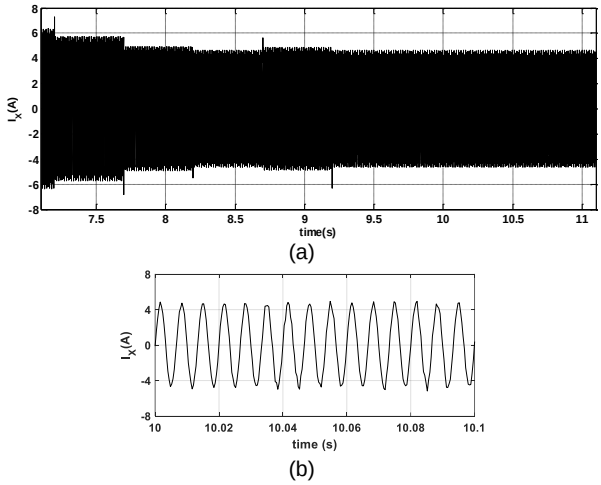

Fig. 11. CW current in the synchronous operation mode (a) and its zoomed (b) waveforms

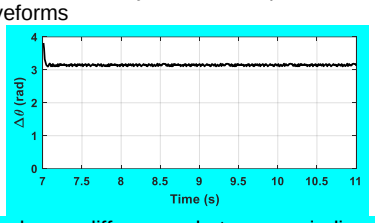

Fig. 12. The phase difference between winding fluxes in the synchronous operation mode

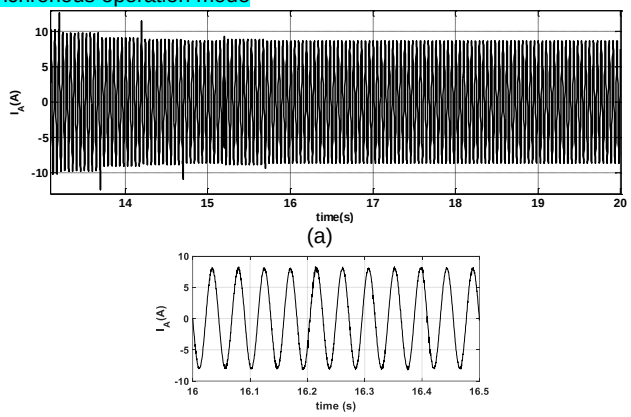

Fig. 13. PW current in the single winding operation mode (a) and its zoomed (b) waveforms

Figure 13 shows the current of the A phase of PW and its zoomed waveforms in the single winding operation mode. The THD of this waveform is 2.73%. Based on the current variations depicted in Figs. 9-13, the search process has been fulfilled in various operation conditions.

Consistent with Figs. 9-13, the stator windings currents are in the permissible range. Accordingly, no overload has been occurred for windings sets.

In order to illustrate the functionality of the proposed DSWIM drive system, some other tests were executed. The efficiency profile for various loads has been determined for proposed torque sharing method (with three modes of operation) and the pervious method proposed in [21-24] (with two modes of operation). Indeed, two scenarios has been regarded:

a) Implementing the torque sharing algorithm given in [21-24] without MTPA
b) Implementing the proposed torque sharing algorithm

without MTPA

Figure 14 (a) illustrates the efficiency profile for various loads for each of these scenarios. In the high loads (higher than the two-pole winding power) both methods are similar and the efficiency is equal in both scenarios. In lower powers, the proposed method in the present paper (with three operation modes) results in higher efficiency. Since, the low power winding is switched off and its power losses is zero. Therefore, in low power condition, the proposed method results in higher efficiency in comparison to the method proposed in [21-24]. In order to investigate the effect of the proposed MTPA strategy on the efficiency improvement, two other scenarios have been considered as follows:

c) Implementing the torque sharing algorithm proposed in [21-24] with the proposed MTPA algorithm.
d) Implementing the proposed torque sharing algorithm with the proposed MTPA algorithm.

Figure 14 (b) illustrates the efficiency for various loads in these two scenarios. Similar to Fig. 14 (a), the efficiency for both scenarios are equal in high load powers as the two methods are similar in load powers higher than the two-pole winding nominal power. Consistent with this figure, the efficiency is higher when the MTPA is implemented with the proposed control system in this paper.

In order to evaluate the proposed MTPA strategy more profoundly and compare its functionality on DSWIMs and IMs, some simulations have been fulfilled. In simulation, the proposed search-based strategy has been implemented on a 3kW IM and a 3.3 kW DSWIM. Table II illustrates the efficiency improvement when the search-based MTPA algorithm is implemented. These tests have been done for various load torques and in the four quadrants of operation regions in the torque-speed plane, when the machine is running at the rated speed. Consistent with this table, the functionality of this strategy is similar in four quadrants. Moreover, as the IM and DSWIM have similar structures and each of the windings of a DSWIM can be considered as an independent IM, the efficiency improvement in approximately the same. In addition, similar to Fig. 13, the efficiency improvement in low load condition is more significant than high loads. As it is expected, the efficiency improvement in the nominal load condition is negligible. Since, in the nominal load, the flux is nominal and cannot be decreased from its rated value. In order to evaluate the parameter sensitivity on the proposed MTPA technique, all of the tests have been repeated in another scenario, in which the value of stator resistances varied 50% from their nominal values. Table III illustrates the Efficiency improvement for this scenario.

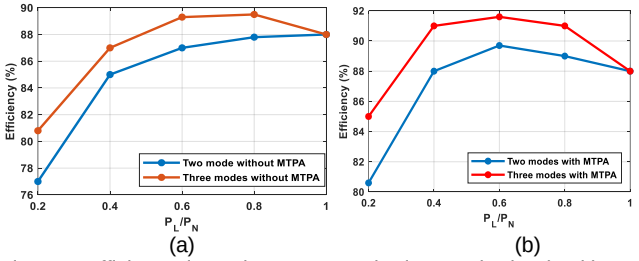

Fig. 14. Efficiency in various torque sharing methods a) with MTPA strategy implementation b) without MTPA strategy implementation

Comparing Tables II and III declares that the results are almost the same and as it was anticipated, the search-based MTPA algorithm is insensitive to machine parameters. Since no machine parameter is utilized for optimal flux calculation and the optimal flux point is determined via a search algorithm free of the machine model and its parameters.

In order to confirm the independency of the proposed MTPA and torque sharing algorithms to the reference frame, it has been also implemented in the rotor flux-oriented reference frame. In this frame, it is assumed that $\lambda'_{qri}=0$ and $\lambda'_{dri}=\lambda'_{ri}$. As a result, the electromagnetic torque produced by each winding set will be as (45).

$$T_{ei}=\frac{3}{4}P_i\frac{L_m}{L'_r}I_{qs1}\lambda'_{ri} \tag{45}$$

For the proposed torque-sharing algorithm in the rotor flux-oriented reference frame, the operation in the synchronous and single winding modes is totally the same as the stator flux-oriented reference frame. However, in the asynchronous operation mode, equation (18) is corrected as (46), based on (45).

$$T^*_{e1}=\frac{3}{4}P_1\left(\frac{L_{m1}}{L'_{r1}}\right)^2\frac{\omega_{sl}\lambda'^*_{r1}}{R'_{r1}}\lambda'^*_{r1} \tag{46}$$

The MTPA algorithm is also similar to that of the stator reference frame, except that, the reference rotor flux is varied stepwisely and the stator current variations is monitored. Figure 15 depicts the efficiency for various loads implementing the proposed MTPA and torque-sharing algorithms both in the stator and rotor flux-oriented reference frames. Consistent with this figure, the results are almost the same for both reference frames, which confirms that the proposed method functionality is independent of reference frame and can be adopted in various reference frames.

VII. Conclusion

An efficient DSWIM drive system was introduced. In this drive system, the torque-sharing between the PW and CW is done based on an innovative and highly efficient algorithm. The proposed algorithm defined three modes of operation for DSWIMs: the asynchronous, single winding and synchronous. The asynchronous operation mode enabled the accurate flux estimation and speed control in zero speed operation region. In the synchronous mode, the torque sharing based on the power rating avoided any overloading of winding sets. Defining the single winding operation mode resulted in DSWIM losses

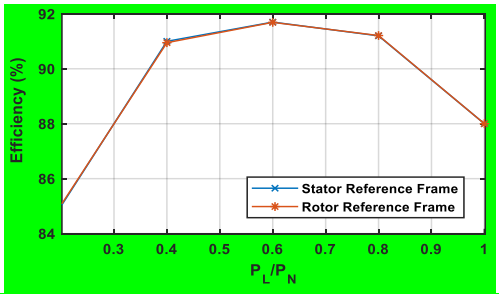

Fig. 15. Efficiency in various reference frames a) stator b) rotor flux

TABLE II
Efficiency improvement implementing the proposed search-based MTPA on a DSWIM and an IM

Operation region	DSWIM				
	$0.2T_N$	**$0.4T_N$**	**$0.6T_N$**	**$0.8T_N$**	**T_N**
Region I ($T>0$ & $\omega_r>0$)	6.57%	4.30%	2.84%	1.66%	Negligible
Region II ($T>0$ & $\omega_r<0$)	6.54%	4.29%	2.82%	1.68%	Negligible
Region III ($T<0$ & $\omega_r<0$)	6.55%	4.31%	2.85%	1.65%	Negligible
Region IV ($T>0$ & $\omega_r<0$)	6.52%	4.30%	2.81%	1.64%	Negligible
Operation region	**IM**				
	$0.2T_N$	**$0.4T_N$**	**$0.6T_N$**	**$0.8T_N$**	**T_N**
Region I ($T>0$ & $\omega_r>0$)	7.23%	4.73%	3.12%	1.84%	Negligible
Region II ($T>0$ & $\omega_r<0$)	7.22%	4.74%	3.10%	1.84%	Negligible
Region III ($T<0$ & $\omega_r<0$)	7.20%	4.71%	3.13%	1.83%	Negligible
Region IV ($T>0$ & $\omega_r<0$)	7.21%	4.75%	3.09%	1.81%	Negligible

TABLE III
Efficiency improvement implementing the proposed search based MTPA on a DSWIM while 50% error in stator resistances

Operation region	$0.2T_N$	$0.4T_N$	$0.6T_N$	$0.8T_N$	T_N
Region I ($T>0$ & $\omega_r>0$)	6.56%	4.30%	2.81%	1.68%	Negligible
Region II ($T>0$ & $\omega_r<0$)	6.57%	4.28%	2.83%	1.62%	Negligible
Region III ($T<0$ & $\omega_r<0$)	6.55%	4.29%	2.84%	1.65%	Negligible
Region IV ($T>0$ & $\omega_r<0$)	6.51%	4.31%	2.82%	1.67%	Negligible

reduction. In addition to implementing a well-organized torque sharing algorithm, a search based MTPA strategy realized in this drive system. The design of this model free MTPA strategy was in coherence with the proposed torque-sharing algorithm. The experimental results of the implementation of the proposed drive system on a 3.3 kW DSWIM confirmed its effectiveness in various operation regions and load conditions.

REFERENCES

[1] H. Abootorabi Zarchi, H. Mosaddegh Hesar and M. Ayaz Khoshhava, "Online Maximum Torque per Power Losses Strategy for Indirect Rotor Flux Oriented Control based Induction Motor Drives," *IET Electric Power Applications*, vol. 13, no. 2, pp. 259-265, Jan. 2019.

[2] S. M. Lu, "A Review of High-Efficiency Motors: Specification, Policy, and Technology", *Renewable and Sustainable Energy Reviews*, vol. 59, pp. 1- 12, June 2016.

[3] I. M. Alsofyani and N. R. N. Idris, "Simple Flux Regulation for Improving State Estimation at Very Low and Zero Speed of a Speed Sensorless Direct Torque Control of an Induction Motor," *IEEE Transactions on Power Electronics*, vol. 31, no. 4, pp. 3027-3035, April 2016.

[4] M. Hajian, J. Soltani, Gh. Arab Markadeh, S. Hosseinnia, "Adaptive Nonlinear Direct Torque Control of Sensorless IM Drives with Efficiency Optimization, " *IEEE Transactions on Industrial Electronics*, vol. 57, no. 3, pp. 975 – 985, March 2010,

[5] A. Munoz-Garcia and T. A. Lipo, "Dual Stator Winding Induction Machine Drive," *33rd IAS Annual Meeting*, St. Louis, MO, USA, pp. 601-608, Oct. 1998.

[6] A. R. Munoz and T. A. Lipo, "Dual stator winding induction machine drive," *IEEE Transactions on Industry Applications*, vol. 36, no. 5, pp. 1369-1379, Sept/Oct. 2000.

[7] M. Ayaz Khoshhava, H. Abootorabi Zarchi and G. Arab Markadeh, "Optimal Design of a Dual Stator Winding Induction Motor with Minimum Rate Reduction Level," *IEEE Transactions on Industrial Electronics*, vol. 68, no. 2, pp. 1016-1024, Feb. 2021

[8] M. Ayaz Khoshhava, H. Abootorabi Zarchi, H. Mosaddegh Hesar, "Direct Torque and Flux Control of Dual Stator Winding Induction Motor Drives based on Emotional Controller", *27th Iranian Conference on Electrical Engineering (ICEE)*, Yazd, Iran, pp. 720-724, Aug. 2019.

[9] J. M. Guerrero and O. Ojo, "Total Airgap Flux Minimization in Dual Stator Winding Induction Machines," *IEEE Transactions on Power Electronics*, vol. 24, no. 3, pp. 787-795, March 2009.

[10] S. Basak and C. Chakraborty, "Dual Stator Winding Induction Machine: Problems, Progress, and Future Scope," *IEEE Transactions on Industrial Electronics*, vol. 62, no. 7, pp. 4641-4652, July 2015.

[11] S. Basak and C. Chakraborty, "A New Optimal Current Control Technique for Dual Stator Winding Induction Generator," *IEEE Journal of Emerging and Selected Topics in Power Electronics*, vol. 5, no. 2, pp. 820-832, June 2017.

[12] Z. Wu, O. Ojo and J. Sastry, "High-Performance Control of a Dual Stator Winding DC Power Induction Generator," *IEEE Transactions on Industry Applications*, vol. 43, no. 2, pp. 582-592, March/April 2007.

[13] J. Sastry, O. Ojo and Zhiqiao Wu, "High Performance Control of a Boost AC-DC PWM Rectifier-Induction Generator System," *40th IAS Annual Meeting*, Hong Kong, China, pp. 1007-1014, Oct. 2005.

[14] S. Chatterjee and S. Chatterjee, "A Novel Speed Sensorless Vector Control of Dual Stator Induction Machine with Space Vector based Advanced 9-zone Hybrid PWM for Grid-connected Wind Energy Generation System," *Electric Power System Research*, vol. 163, pp. 174–195, Oct. 2018.

[15] O. Ojo and Z. Wu, "Speed Control of a Dual Stator Winding Induction Machine," *22nd Annual IEEE Applied Power Electronics Conference and Exposition*, Anaheim, CA, USA, pp. 229-235, March 2007.

[16] Z. Wu, O. Ojo and G. Dong, "MRAS Speed Estimation and Full-Order Flux Observer for Dual Stator Winding Induction Motor Drives," *IEEE Power Electronics Specialists Conference*, Orlando, FL, USA, pp. 2428-2434, June 2007.

[17] J. M. Guerrerot and O. Ojo, "Performance Optimization in Dual Stator Winding Induction Machines through Flux Partitioning," *4th IET Conference on Power Electronics, Machines and Drives*, York, pp. 696-700, April 2008.

[18] J. M. Guerrero; O. Ojo, "Flux Level Selection in Vector-Controlled Dual Stator Winding Induction Machines," *IET Electric Power Applications*, vol. 3, no. 6, pp. 562–572, Dec. 2009.

[19] J. M. Guerrero and O. Ojo, "Air Gap Flux Density Optimization in Dual Stator Winding Induction Machines," *IEEE Power Electronics Specialists Conference*, Rhodes, Greece, pp. 3767-3773, June 2008.

[20] M. Ayaz Khoshhava, H. Abootorabi Zarchi and G. R. Arab Markadeh, "Optimal Reference Frame Angle Approach for Air-Gap Flux Minimization in Dual Stator Winding Induction Machines," *IEEE Transactions on Power Electronics*, vol. 35, no. 7, pp. 6658-6662, July 2020.

[21] M. A. Khoshhava, H. Abootorabi Zarchi and G. A. Markadeh, "Sensorless Speed and Flux Control of Dual Stator Winding Induction Motors Based on Super Twisting Sliding Mode Control," *IEEE Transactions on Energy Conversion*, vol. 36, no. 4, pp. 3231-3240, Dec. 2021.

[22] M. Ayaz and H. Abootorabi, "Direct Torque Control of Dual Stator Winding Induction Machine Based on PI-Sliding Mode Control," 26th *Iranian Conference on Electrical Engineering (ICEE)*, Mashhad, Iran, pp. 1233-1239, May 2018.

[23] M. Vazifedan, H. Abootorabi Zarchi and M. A. Khoshhava, "Sensorless Control of Dual Stator Winding Induction Machine Drive Using Sliding Mode Control Based Model Reference Adaptive System," *11th Power Electronics, Drive Systems, and Technologies Conference (PEDSTC)*, Tehran, Iran, pp. 1-7, Feb. 2020.

[24] M. Vazifehdan, H. Abootorabi Zarchi and M. A. Khoshhava, "Sensorless Vector Control of Induction Machines via Sliding Mode Control based Model Reference Adaptive System," *28th Iranian Conference on Electrical Engineering (ICEE)*, Tabriz, Iran, pp. 1-6, Aug. 2020.

Mojtaba Ayaz Khoshhava received M.S. and Ph.D. from Shiraz University and Ferdowsi University of Mashhad in 2014 and 2020, respectively. He is currently a postdoctoral fellow at École de Technologie Supérieure (ÉTS).

His main research interests include electrical machines control, design and modeling.

Hossein Abootorabi Zarchi received the M.S. and Ph.D. degrees in Electrical Engineering from the Isfahan University of Technology, Isfahan, Iran, in 2004 and 2010, respectively.

He is currently an Assistant Professor in the Department of Electrical Engineering, Ferdowsi University of Mashhad, Mashhad, Iran. His research interests include electrical machines, nonlinear control of motor drives, and renewable energies.

Gholamreza Arab Markadeh received the B.Sc., M.Sc., and Ph.D. degrees in Electrical Engineering from Isfahan University of Technology, Iran, in 1996, 1998, and 2005, respectively. He is currently an Associate Professor in the Faculty of Engineering, Shahrekord University, Shahrekord, Iran. Since January 2021, he has been cooperating as a Lecturer with the Faculty of Engineering, Ferdowsi University of Mashhad, Mashhad, Iran.

His fields of research include nonlinear control, power electronics, and variable-speed drives.

Hamidreza Mosaddegh received the M.Sc. and Ph.D. degrees in Electrical Engineering from Ferdowsi University of Mashhad, Iran, in 2014 and 2019, respectively. His current interests include control of high-performance drives, modelling of electrical machines, and renewable energies.

Kamal Al-Haddad (S'82-M'88-SM'92-F'07, LF'20) received the B.Sc.A. and M.Sc.A. degrees from the University of Québec à Trois-Rivières, Canada, in 1982 and 1984, respectively, and the Ph.D. degree from the Institute National Polythechnique, Toulouse, France, in 1988. Since June 1990, he has been a Professor with the Electrical Engineering Department, École de Technologie Supérieure (ETS), Montreal, QC, where he has been the holder of the senior Canada Research Chair in Electric Energy Conversion and Power Electronics since 2002. He is a consultant and has established very solid link with many Canadian industries working in the field of power electronics, electric transportation, aeronautics, and telecommunications. He successfully transferred and implemented 26 technologies to Canadian and international compagnies. His fields of interest are in highly efficient static power converters, harmonics and reactive power control using hybrid filters, voltage level multiplier, resonant and multilevel converters including the modeling, control, and development of prototypes for various industrial applications in electric traction, renewable energy, power supplies for drives, telecommunication, etc. Prof. Al-Haddad is a member of the Academy of Sciences and fellow of the Royal Society of Canada and a fellow member of the Canadian Academy of Engineering. He is IEEE IES President 2016-2017, Associate editor of the Transactions on Industrial Informatics, IES Distinguished Lecturer and recipient of the 2014 IEEE IES Dr.-Ing. Eugene Mittelmann Achievement Award. He has been elected the IEEE 2022 division VI director elect.